# Structure−Property Relationships in Organic−Inorganic Nanomaterials Based on Methacryl−POSS and Dimethacrylate Networks

**Stéphane Bizet, Jocelyne Galy,* and Jean-François Gérard**

*Laboratoire des Matériaux Macromoléculaires/IMP UMR CNRS 5627, Institut National des Sciences Appliquées de Lyon, Bât Jules Verne-20 Av. A. Einstein, F-69621 Villeurbanne Cedex, France*

*Received July 19, 2005; Revised Manuscript Received January 25, 2006*

ABSTRACT: Dimethacrylate-based networks were modified with well-defined organic−inorganic building blocks, i.e., polyhedral oligomeric silsesquioxanes (POSS). POSS were incorporated in the polymer networks either as dangling chains or as cross-linking points. For this purpose, the POSS functionality was varied. The influence of the structure of the organic substituent of the POSS cage was also investigated. The structure of the POSS-modified networks was determined by WAXS, TEM, and thermomechanical analysis. The POSS as a pendant unit on the network backbone shows a strong tendency toward aggregation and crystallization, depending on the nature of the organic ligands. The POSS−POSS interaction was found to be the main parameter governing the network morphology. However, dynamic mechanical properties remain nearly at the same level as the neat matrix. Multifunctional POSS shows a higher miscibility with the dimethacrylate monomer and disperses very well in the cured network. As expected, the rubbery modulus grows with increasing amounts of POSS according to the high functionality of these additional cross-links, whereas the glass transition temperature remains constant. It is also demonstrated that if the polymerization occurs at high temperature, the distribution of relaxation times is reduced and more homogeneous hybrid networks, in terms of molecular mobility, are obtained.

## Introduction

For the last decade, organic−inorganic hybrid nanocomposites based on the incorporation of polyhedral oligomeric silsesquioxanes or POSS into polymeric matrices have received a considerable amount of attention. POSS have a compact hybrid structure with an inorganic core made up of silicon and oxygen $(SiO_{1.5})_n$ (with $n = 8$, 10, and 12) externally surrounded by nonreactive or reactive polymerizable organic ligands.[1,2] The interaction between the organic ligand and the matrix controls the degree of dispersion of POSS in the medium, i.e., its compatibility, and thus the final properties of the POSS-modified polymers. POSS can be dispersed on a molecular level (1−3 nm) or as aggregates (crystalline or amorphous), which can be on the order of micrometers in size. In the case of functional POSS which can be covalently bonded to the polymer backbone, the length scale of association may be reduced.

Both monofunctional and multifunctional POSS have been used to modify thermosetting materials and most of the papers published are related to epoxy-based networks.[3−13] Only a few studies concern dimethacrylate-based networks.[14−19] Depending on its functionality, POSS can be incorporated as a pendant unit in the network if it bears only one reactive group, or POSS can be incorporated as a junction (cross-linking point) if it bears more than two reactive groups.

In this study, two types of monofunctional methacryl−POSS and one multifunctional methacryl−POSS were incorporated into dimethacrylate-based networks through radical-initiated copolymerization with organic methacrylate monomers.[16−18] The main applications of dimethacrylate-based networks can be found in dental restorative materials, photolithography, information-storage systems, coatings, photonics, and ophthalmic lenses. It is well-known that unmodified dimethacrylate-based networks are highly heterogeneous. This structural heterogeneity is inherent in the polymerization process. The formation of microgels in the early stage of the reaction is the primary cause of structural heterogeneity of the network.[20−26] Microgels are densely cross-linked and cyclized polymers. Microgels result from the formation of a highly cross-linked region near the site of the initiated radical. Gelation occurs when microgels have grown and connected, resulting in a macroscopic network. As a consequence, at a very low conversion, the polymerization passes from chemical control to diffusion control, so that the final double bond conversion, the polymerization rate, and the network structure depend only on the network mobility and hence on the temperature and monomer structure. The structural heterogeneity of dimethacrylate-based networks has been demonstrated through the characterization of relaxation times (by dynamic mechanical spectroscopy) and morphology (by transmission electron microscopy and atomic force microscopy). Before gelation, the microgel size was measured using dynamic light scattering. The copolymerization between a methacrylate-based monomer and a methacryl-based POSS leads to a more complex situation. Indeed, an additional important parameter is the reactivity ratio of the two monomers. In a mixture of methyl methacrylate (MMA) and methacryl-based POSS, it was shown that the reactivity ratio, $r_{POSS}$, is below one while the reactivity ratio of MMA, $r_{MMA}$, is above 1.[27] These values are also dependent on the nature of the organic substituent of the POSS cage. It means that monofunctional methacryl-based POSS are slightly less reactive than classical methacrylate-based monomers.

The objective of this work is to determine how these functionalized POSS and the structure of the organic substituent on the inorganic cage will affect the compatibility, the morphologies and the final properties of methacrylate-based networks. For this purpose, the microstructure of the POSS-modified networks was characterized by wide-angle X-ray scattering (WAXS), transmission electron microscopy (TEM), and dynamic mechanical analysis (DMA).

* Corresponding author. E-mail: jocelyne.galy@insa-lyon.fr.

10.1021/ma051574x CCC: $33.50 
Published on Web 03/08/2006

**Scheme 1. Chemical Structure of the POSS Monomers and Organic Monomers Used in This Study**

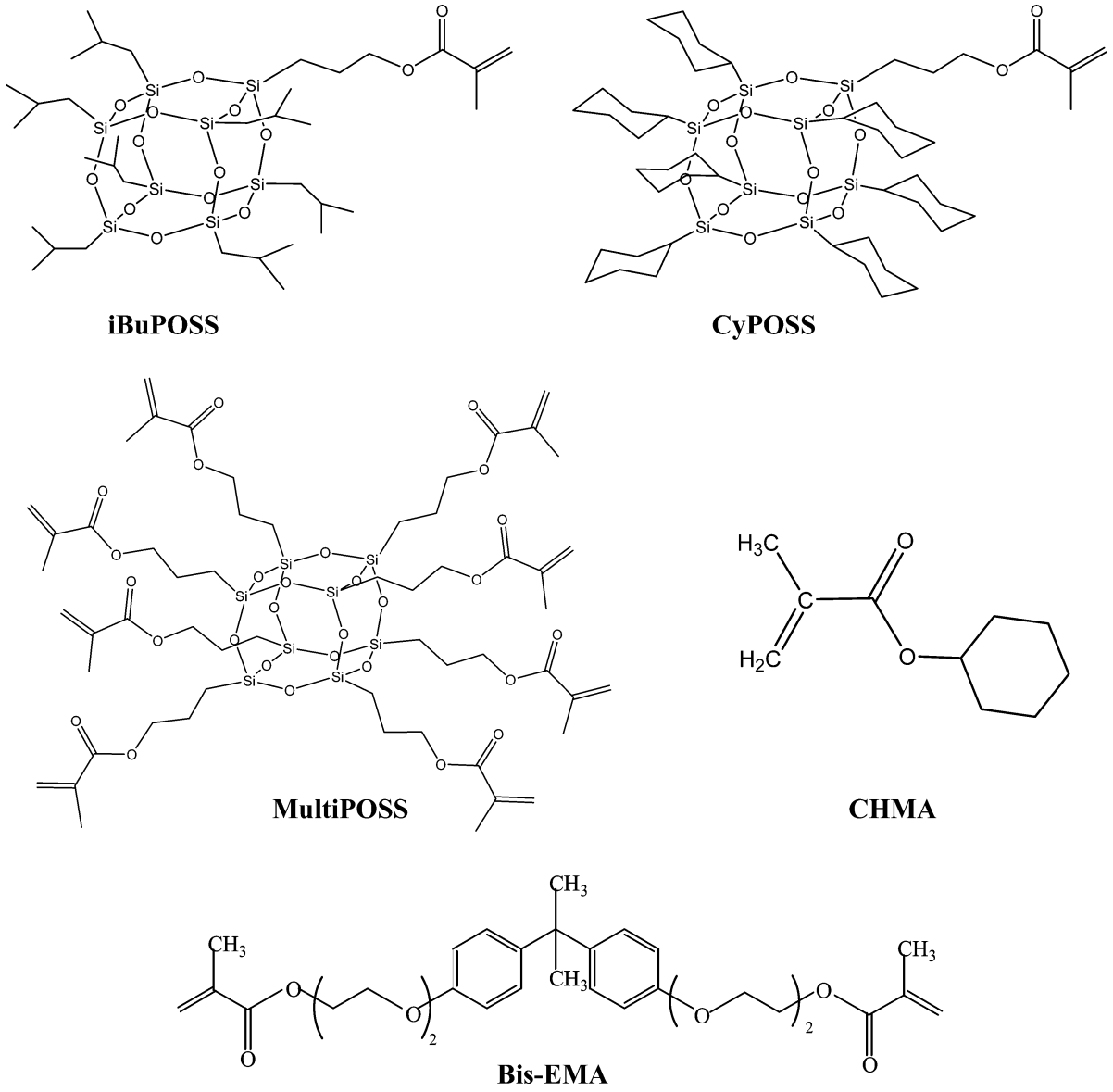


## Experimental Section

**Materials.** (Isobutyl)$_7$Si$_8$O$_{12}$(propyl methacrylate) and (cyclohexyl)$_7$Si$_8$O$_{12}$(propyl methacrylate), denoted $^i$BuPOSS and CyPOSS respectively, and (propyl methacrylate)$_8$Si$_8$O$_{12}$, denoted multiPOSS, were purchased from Hybrid Plastics[27] (Hattiesburg, MS). $^i$BuPOSS and CyPOSS are crystalline compounds ($T_m$ = 109 °C for $^i$BuPOSS whereas no fusion was observed before degradation for CyPOSS) while multiPOSS is an amorphous compound. MALDI−TOF and $^{29}$Si NMR spectroscopies reveal that $^i$BuPOSS and CyPOSS have a pure $T_8$ core whereas MultiPOSS is a complex mixture of structures ranging from $T_8$ to $T_{12}$. $^i$BuPOSS and MultiPOSS were used as received, but CyPOSS was purified by recrystallization from methanol in order to remove residual trisilanol POSS that was found by MALDI−TOF and $^{29}$Si NMR spectroscopies.[16] Cyclohexyl methacrylate denoted CHMA, from Aldrich and tetra ethoxylated bisphenol A dimethacrylate, denoted Bis-EMA, from Cray Valley Co., were used as received. Azobis(isobutyronitrile) free radical initiator, AIBN, and *tert*-butyl peroxide, $^t$BPO, were purchased from Aldrich and were used as received. Chemical structures of all monomers used in this study are shown in Scheme 1.

**Network Synthesis. POSS Cages as Dangling Objects.** Samples were prepared by adding 5−10 wt % of monofunctional POSS to a mixture of CHMA/Bis-EMA ((100 − $x$)/$x$) where $x$ ranges from 0 to 50 wt %. The solubility of $^i$BuPOSS into Bis-EMA is weak: for 1 wt % of POSS, the temperature must be higher than 45 °C to have a homogeneous mixture, and for 5 wt %, the temperature must be above 90 °C. The solubility of CyPOSS is worse even at low concentrations: for 1 wt % of POSS the temperature needed to have a homogeneous mixture is above 130 °C.[16] This clear difference of solubility between $^i$BuPOSS and CyPOSS is due to the difference of interactions developed between the clusters forming crystalline structures. Therefore, to improve the solubility of these monofunctional POSS monomers, we used CHMA as a reactive solvent. The three monomers (Bis-EMA, CHMA, and POSS) and AIBN (0.5 wt %) were mixed at room temperature. After degassing under argon to remove oxygen which inhibits the free radical polymerization, the homogeneous mixture was poured into a 1 mm thick mold, made of two glass plates. All samples were cured at 65 °C for 8 h followed by a post-curing at 130 °C for 2 h. An example of a typical polymer repetitive unit is illustrated in Scheme 2.

**POSS Cages as Cross-Links.** Samples based on multifunctional POSS were prepared by blending 5, 10, or 15 wt % of multiPOSS into Bis-EMA. It was not necessary in that case to use a reactive diluent because of the high solubility of this POSS into the organic monomer. This is due to the presence of the eight methacrylate groups which interact favorably with Bis-EMA. AIBN (0.5 wt %) was used. The curing cycle was 8 h at 80 °C (due to the lower

**Scheme 2. Example of a Possible Structural Unit in Nanocomposites**

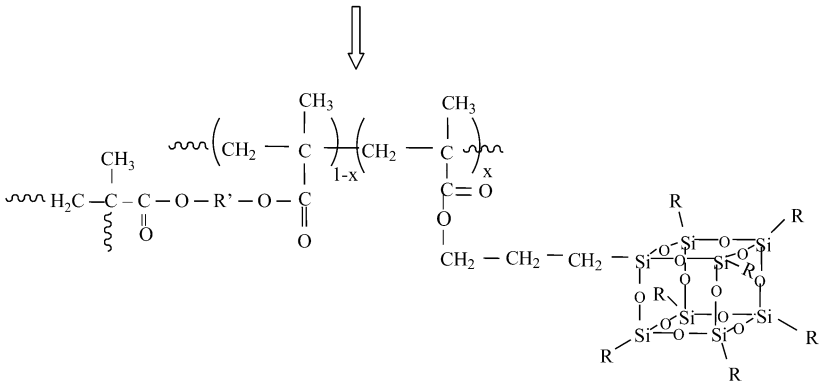


reactivity of multiPOSS, a higher temperature of curing was needed) followed by a post-curing at 150 °C for 2 h. Some networks were also synthesized using 0.5 wt % of $^t$BPO. In that case the curing cycle was 4 h at 130°C in order to obtain a reaction kinetics in the same range as with AIBN.

**Infrared Spectroscopy.** Double bond conversion was measured by Near Infra-Red spectroscopy on a Bruker Equinox 55 spectrometer, using the absorption band at 6163 $cm^{-1}$ associated with the vinyl methacrylate functions.[28] As the double bond from POSS, CHMA, or Bis-EMA cannot be distinguished by this technique, the values reported later correspond to the whole methacrylate conversion. The reference band used for the calculation was the CH band from the aromatic cycles at 4624 $cm^{-1}$.[28] Conversions were calculated from the Beer−Lambert law.

**X-ray Scattering.** Wide-angle X-ray diffraction (WAXS) was carried out on a Siemens D500, at room temperature. Cu Kα radiation was used.

**Transmission Electron Microscopy.** A Phillips CM12 transmission electron microscope was used to characterize the morphology of the nanocomposites. The specimens used were microtomed to an approximate thickness of 100 nm and were set on a copper grid.

**Dynamic Mechanical Spectroscopy.** Viscoelastic properties were analyzed using a RSA II rheometer from Rheometric Co. Samples were tested in tensile mode applying a dynamic strain of 0.05% at 1 Hz. Storage modulus and loss modulus, $E'$ and $E''$ respectively, and tanδ were measured as a function of temperature from −130 to +180 °C at a heating rate of 4 °C/min. Samples were approximately 30 × 5 × 1 $mm^3$.

Master curves were obtained by applying the time−temperature equivalence principle from a reference temperature ($T_0$), chosen close to Tα (at 1 Hz). Storage and loss moduli were measured on temperature steps (each 5 °C from Tα − 50 °C to Tα + 50 °C) for various frequencies ranging from 0.1 to 100 rad·$s^{-1}$. For each isothermal recording, a shift factor $a_T$ was obtained from $E'$ and $E''$ in order to get master curves, i.e., $E'$ and $E''$ vs frequency at $T_0$. Any vertical correction was done. Then, the set of $a_T$ values was used to build the $E'$ master curve and compute $C_0^1$ and $C_0^2$, the WLF coefficients according to the WLF equation.

## Results and Discussion

**1. Structure of Networks with POSS as Dangling Object.** WAXS profiles for the $^i$BuPOSS-modified Bis-EMA/CHMA networks and CyPOSS-modified Bis-EMA/CHMA networks are shown in Figure 1 and Figure 2, respectively.

One can see in Figure 1, parts d and a, sharp crystalline peaks of the pure $^i$BuPOSS and the amorphous halo of the neat Bis-EMA/CHMA matrix, respectively. The diffractogram of the 5 wt % $^i$BuPOSS-filled network (Figure 1b) shows a unique peak at $2\theta = 8.25°$ ($d = 10.68$ Å) and the amorphous halo. Increasing the amount of $^i$BuPOSS up to 10 wt % causes the intensity of the peak at $2\theta = 8.25°$ to increase (Figure 1c). Weaker reflections at $2\theta = 11.1°$, 12.3°, 19.2° are also observed on the diffractogram. This proves that appreciable POSS crystallinity is present within the polymer network, especially at a loading of 10 wt %. The size of crystallites, determined from the full width at half-maximum of the peak, thanks to the Debye-Sherrer formula, is in the range of 60−70 nm. So cross-linking does not suppress crystallinity. However, the comparison of the peak position of the pure $^i$BuPOSS to the modified network reveals that the POSS crystal structure is affected by the incorporation in the organic matrix. The main reflections of $^i$BuPOSS crystal at $2\theta = 8.1$, 10.2, 11.8, and 18.8° do not match those of the filled network and the reflection at $2\theta = 7.5°$ is not present in the modified material as well.

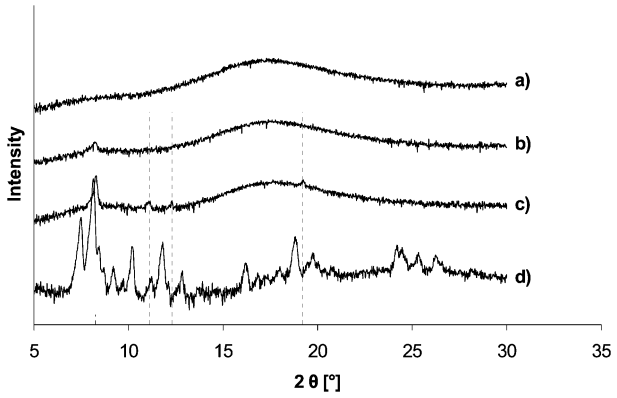


**Figure 1.** WAXS patterns: (a) Bis-EMA/CHMA (50/50); (b) Bis-EMA/CHMA (50/50) + 5 wt % $^i$BuPOSS; (c) Bis-EMA/CHMA (50/50) + 10 wt % $^i$BuPOSS; (d) $^i$BuPOSS.

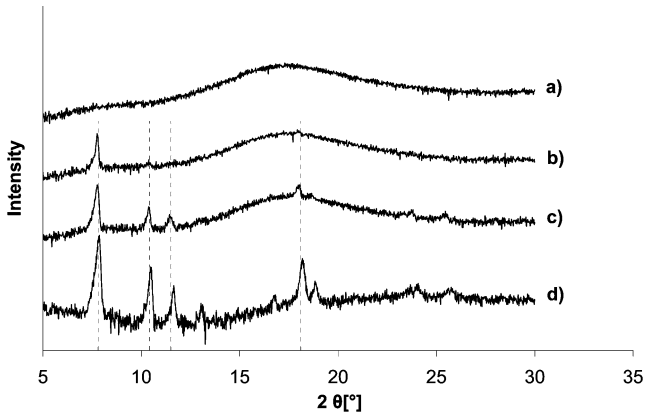


**Figure 2.** WAXS patterns: (a) Bis-EMA/CHMA (50/50); (b) Bis-EMA/CHMA (50/50) + 5 wt % CyPOSS; (c) Bis-EMA/CHMA (50/50) + 10 wt % CyPOSS; (d) CyPOSS.

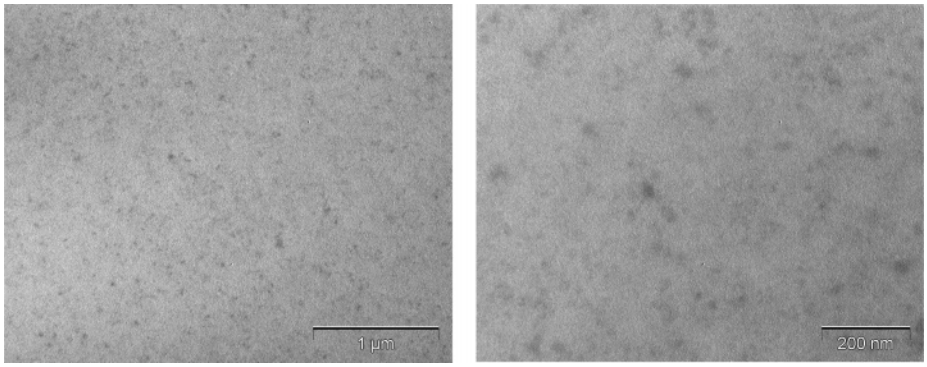


**Figure 3.** TEM micrographs of the Bis-EMA/CHMA (50/50) + 10 wt % $^{i}$BuPOSS network at two magnifications.

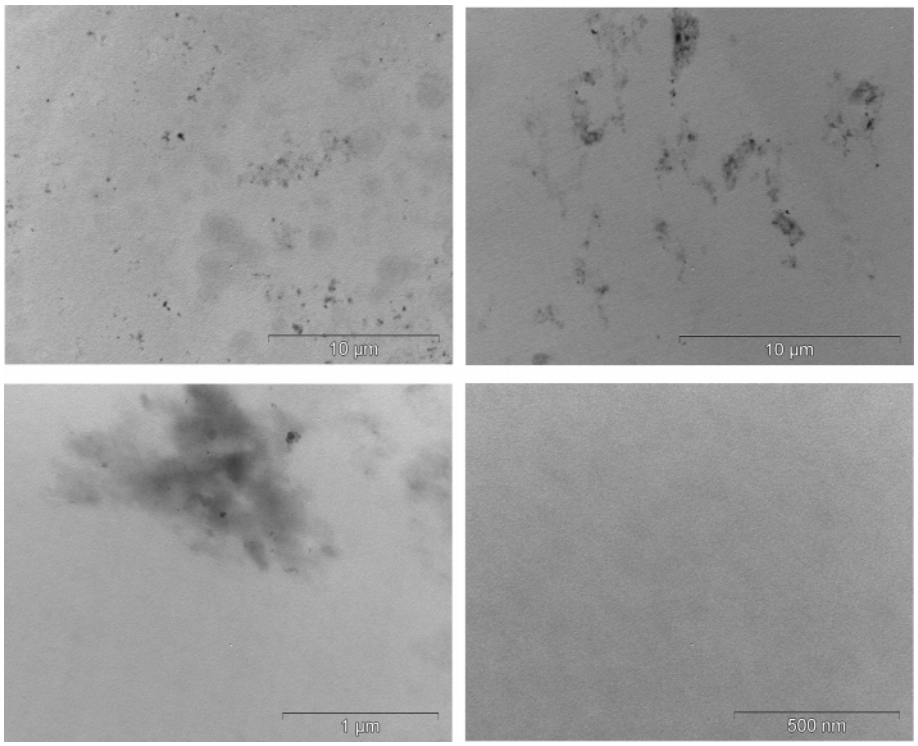


**Figure 4.** TEM micrographs of the Bis-EMA/CHMA (50/50) + 5 wt % CyPOSS network at different magnifications.

Very different behavior is observed on CyPOSS-based networks (Figure 2). There is a strong correspondence between the peak patterns of the networks and pure CyPOSS. The four main reflection peaks of CyPOSS at $2\theta = 7.8$, 10.41, 11.5, and 18° are retrieved in the two CyPOSS-based networks. So, one can conclude that the crystal structure of CyPOSS is not affected by the incorporation in the network. The size of the crystalline domains is estimated to be equal to 100−120 nm.

The comparison of the spectrum of Bis-EMA/CHMA (50/50) + 5 wt % $^{i}$BuPOSS to the spectrum of Bis-EMA/CHMA (50/50) + 5 wt % CyPOSS (Figure 1b and Figure 2b) indicates a lower amount of crystallinity and a better dispersion of the $^{i}$BuPOSS as compared to CyPOSS. Moreover the simple naked eye examinations of the samples show that $^{i}$BuPOSS-based networks are transparent while CyPOSS-based networks are opaque even for a 5 wt % loading. It is clear that the monofunctional POSS bearing seven cyclohexyl groups has a great tendency to aggregate within the methacrylate polymer matrix during the polymerization process.

The TEM micrographs of the POSS-filled networks, reported in Figures 3 and 4, show dark zones that correspond to the POSS-rich zones (higher electron density due to the presence of silicon atoms). A uniform and fine dispersion of domains is observed in Bis-EMA/CHMA (50/50) + 10 wt % $^{i}$BuPOSS network (Figure 3); the domain size about 50 nm is in agreement with the conclusions from WAXS analyses. Because of the fact that the crystalline structure of $^{i}$BuPOSS incorporated in the network is not the same as the pure POSS, we suggest that the POSS, which is initially soluble in the monomer mixture, phase separates from the reactive organic medium because its solubility in the organic medium becomes lower during the polymerization. Moreover, kinetic reasons may be evoked; the reactivity of methacrylate POSS is likely to be lower compared to that of Bis-EMA and CHMA due to steric hindrance.[17,27] Thus, the slower incorporation of POSS into the network may contribute to the phenomenon of phase separation (higher concentration of $^{i}$BuPOSS in the sol phase).

Numerous POSS-rich domains are visible in the Bis-EMA/CHMA (50/50) + 5 wt % CyPOSS network (Figure 4). In contrast to the previous network, the dispersion of these domains is heterogeneous and coarse. Most of the aggregates have a size of about 1 $\mu$m and their structure is not well-defined. Substructure between a few hundreds and a few tens of nanometers can be seen. No POSS-rich phase could be observed at high magnification, unlike the $^{i}$BuPOSS-based network. Two parameters may explain this behavior: (i) the low solubility of

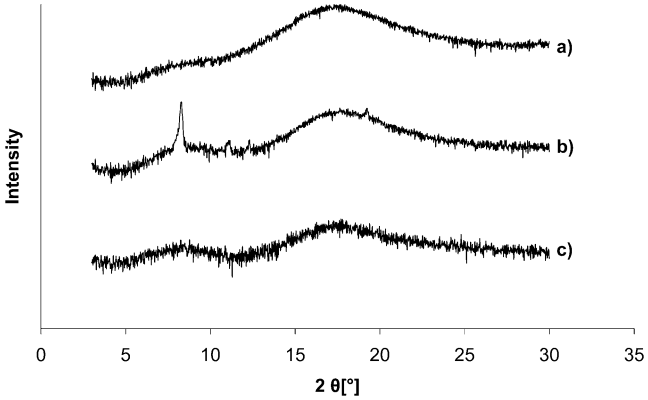


**Figure 5.** WAXS patterns: (a) Bis-EMA/CHMA (50/50); (b) Bis-EMA/CHMA (50/50) + 10 wt % *i*BuPOSS; (c) Bis-EMA/CHMA (50/50) + 10 wt % *i*BuPOSS after extraction of free POSS by THF.

**Table 1. Final Double Bond Conversion Measured by NIR Spectroscopy, after Curing of Networks**

| | bis-EMA/CHMA (50/50) | bis-EMA/CHMA + 5 wt % POSS | bis-EMA/CHMA + 10 wt % POSS |
|---|---|---|---|
| *i*BuPOSS | 86 | 83 | 85 |
| CyPOSS | 86 | 84 | 82 |

CyPOSS in the organic medium even if the initial mixture seems homogeneous (transparent) at room temperature and (ii) the strong tendency of these POSS molecules to aggregate because of the very favorable CyPOSS−CyPOSS interactions.

A very important question arising is whether all the POSS are covalently linked to the network, because we know from the infrared spectroscopy that the final double bond conversion does not reach 100% (Table 1): only 82−85% of double bonds have reacted during polymerization. The hybrid network (Bis-EMA/CHMA (50/50) + 10 wt % POSS) has been washed by THF for 72 h in a Soxhlet apparatus. Then an elemental analysis of the washed material was carried out and the amount of extracted POSS calculated; it appears that of the 10 wt % of either POSS monomer initially added to the organic monomers, 5 wt % of *i*BuPOSS and only 2 wt % of CyPOSS are covalently linked to the network. The WAXS profiles corresponding to the extracted network are shown in Figure 5. It reveals only a broad amorphous maximum at $2\theta \approx 8°$, instead of the sharp crystalline reflection at $2\theta = 8.3°$. This maximum is assumed to be characteristic of intermolecular packing as such an amorphous halo is observed for the material before extraction (Figure 5b) or for the pure matrix (Figure 1a). We can infer that most of POSS present in phase-separated crystals have been removed from the material. In our hybrid networks we will now consider that there are two kinds of POSS: those covalently bonded to the network and acting as pendant objects, and those which are aggregated into inorganic crystalline domains of various sizes, but not chemically bound to the matrix, which behave as a filler.

Additionally, the influence of the amount of reactive solvent, MCHA, used in the monomer mixture and the influence of the post-curing step have been examined. Figure 6 shows that the *i*BuPOSS does not organize itself in the same way depending on the proportion of CHMA with respect to Bis-EMA. Three WAXS profiles, corresponding to three different hybrid I/O networks based on *i*BuPOSS without post-curing, are reported:

(i) The linear copolymer (CHMA + 10 wt % *i*BuPOSS, Figure 6c) is fully amorphous and exhibits a broad maximum at $2\theta = 8.5°$, this maximum is also observed in the neat poly(cyclohexyl methacrylate) polymer and is attributed to the intermolecular organization of the polymer chains.[30] Therefore,

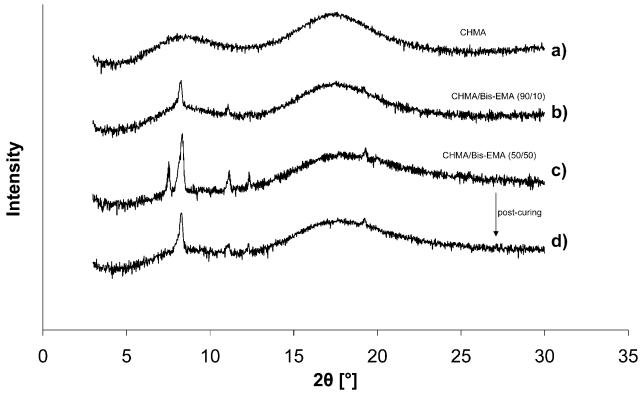


**Figure 6.** WAXS patterns: (a) CHMA + 10 wt % *i*BuPOSS; (b) Bis-EMA/CHMA (10/90) + 10 wt % *i*BuPOSS; (c) Bis-EMA/CHMA (50/50) + 10 wt % *i*BuPOSS, after curing 8 h at 65 °C; (d) Bis-EMA/CHMA (50/50) + 10 wt % *i*BuPOSS, after post-curing 2 h at 130 °C.

one can conclude that *i*BuPOSS molecules are individually dispersed.

(ii) As soon as 10 wt % of Bis-EMA is introduced in the organic monomer mixture (Figure 6b) some POSS crystals appear during the first step of the curing cycle (8 h at 65 C°) as the clusters phase separate during the polymerization

(iii) Increasing the amount of Bis-EMA (Figure 6a) reduces the solubility of POSS, and as a consequence, more crystallinity is observed. Sharp peaks at $2\theta = 8.3$ and 7.5° are observed.

The post-curing cycle (2 h at 130 °C) modifies the morphology of the POSS in the polymer network (Figure 6d): the intensity of the peak at 8.3° decreases and the peak at 7.5° disappears. It means that the number of crystallites decreases after the post-curing step. The crystalline organization of the clusters is unchanged after post-curing as shown by the fact that the peaks at $2\theta = 8.3$, 11.1, and 12.3° are still present. In fact, 130 °C is above the melting temperature of *i*BuPOSS crystallites ($T_m = 109$ °C), so the crystalline organization is broken during the post-curing step and probably some of these clusters are able to diffuse and to react with surrounding trapped radicals.

In the case of CyPOSS, no significant difference in the WAXS pattern can be seen whatever the amount of CHMA or the application of post-curing. All the WAXS patterns were similar to the one reported in Figure 2c, i.e., in all cases crystalline domains are observed. This result underlines the very strong influence of the nature of the nonreactive organic substituents of monofunctional POSS (isobutyl vs cyclohexyl) on the miscibility of POSS molecules in an organic medium and on the interaction energy between clusters in crystalline structures built from *i*BuPOSS or CyPOSS. An example of the microstructure of a POSS-modified dimethacrylate network is represented in Scheme 3 in an idealized two-dimensional schematic representation: covalently bonded POSS, and crystalline POSS particles and amorphous aggregates are shown.

The dynamic mechanical analysis was conducted on the two hybrid networks (Bis-EMA/CHMA (50/50) + 10 wt % *i*BuPOSS and Bis-EMA/CHMA (50/50) + 10 wt % CyPOSS) and compared to the reference fully organic network (Bis-EMA/CHMA (50/50)). Variations of $G'$ and tan $\delta$ as a function of temperature are reported in Figure 7, parts a and b. No large difference is observed between the two different types of networks: the main relaxation at high temperature, $T\alpha$, taken as the maximum of tan $\delta$ peak and associated with the glass transition, and the sub-$T_g$ relaxation near −80 °C, associated with the change of conformations of cyclohexyl groups in the monomer units[31] occur at the same temperatures. So, the effects

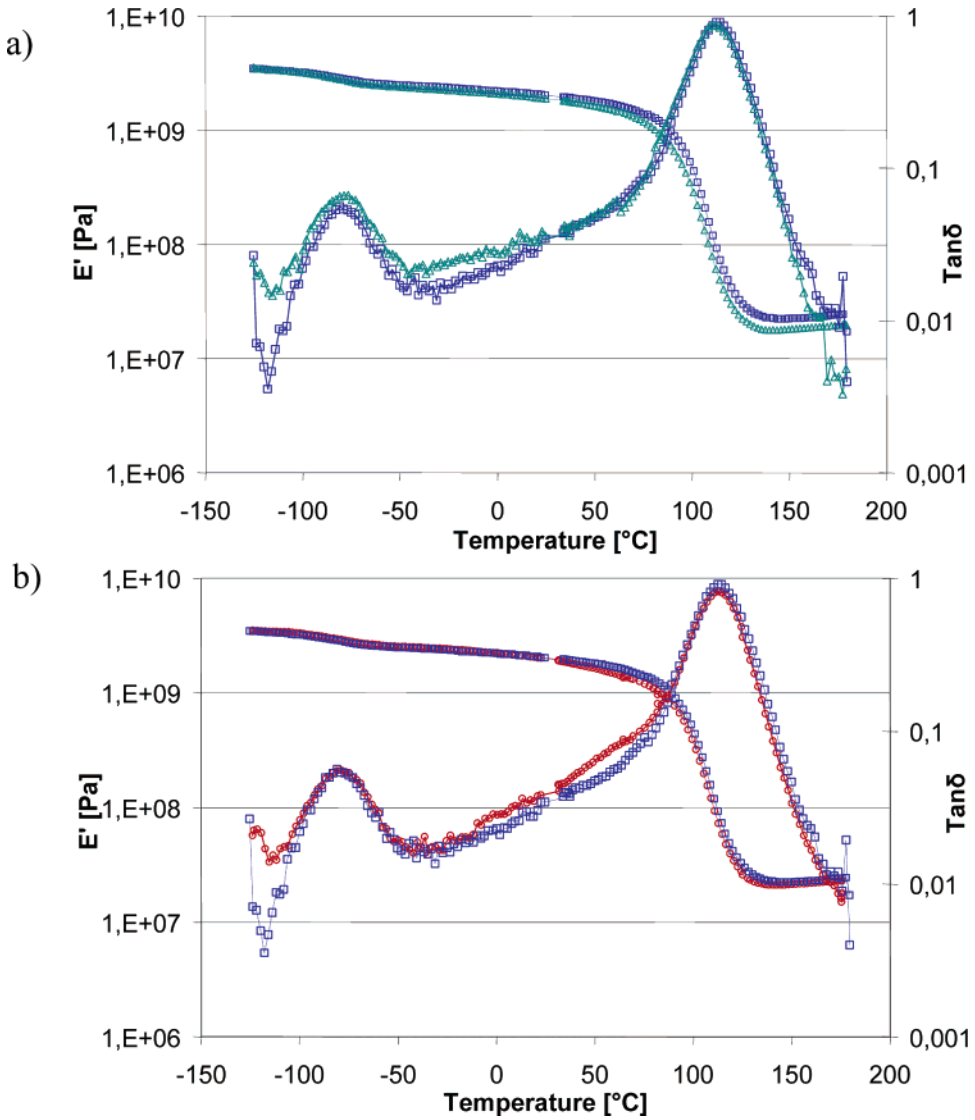


**Figure 7.** Storage modulus, $G'$, and loss factor, tan $\delta$, of at 1 Hz: (a) Bis-EMA/CHMA (50/50) + 10 wt % $^{i}$BuPOSS (△) and Bis-EMA/CHMA (50/50) (□); (b) Bis-EMA/CHMA (50/50) + 10 wt % CyPOSS (○) and Bis-EMA/CHMA (50/50) (□)

**Scheme 3. Schematic Representation of the Structure of a Network Based on Bis-EMA/CHMA/Methacryl−POSS[a]**

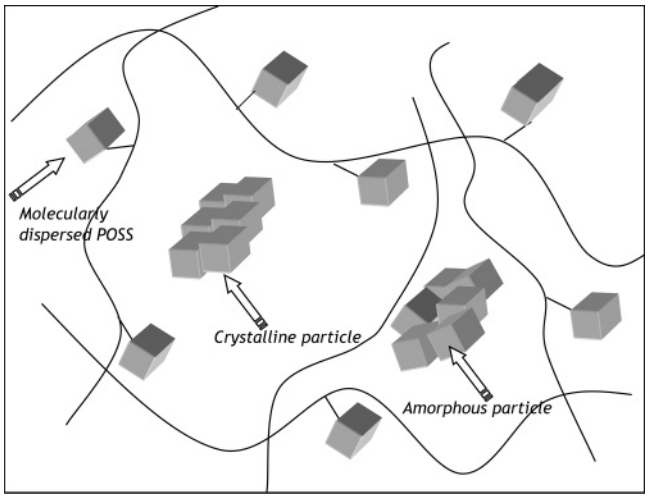


[a] Solid lines represent the organic polymer chains; POSS can be found in three different states: molecularly dispersed, amorphous, and crystalline particles.

of the nature of substituents of the inorganic POSS core remain minor on these viscoelastic properties. Only a slight decrease of the rubbery modulus is observed as 10 wt % of $^{i}$BuPOSS is added to the organic medium; it is accompanied by a 3 °C decrease of $T\alpha$ (from 113 °C for the reference network to 110 °C for the hybrid network, Table 3). The same trend is observed for CHMA/Bis-EMA (90/10) + POSS networks. Incorporation of 10 wt % of $^{i}$BuPOSS leads to a decrease of $T\alpha$ (6 °C lower than the reference network) and of the rubbery modulus as compared to the pure matrix. At the same time, 10 wt % of CyPOSS let $T\alpha$ and the rubbery modulus unchanged (Table 3).

To highlight the effect of POSS on the network structure, master curves $E'$ and $E''$ as a function of frequency were built for each material. Figure 8 shows master curves of both the Bis-EMA/CHMA(50/50) + 10 wt % $^{i}$BuPOSS network and the reference matrix. The superimposition of isothermal curves to build those master curves confirms the validity of time−temperature equivalence principle for the materials studied. The evolution of the shift factor $a_T$ in the temperature window considered was estimated according to the WLF equation, eq 1:[32]

$$\log (a_T) = \frac{-C^0_1(T - T_0)}{C^0_2 + (T - T_0)} \quad (1)$$

WLF parameters, $C^0_1$ and $C^0_2$, at the reference temperature, $T_0$,

**Table 2. Final Double Bond Conversion Measured by NIR Spectroscopy**

| | bis-EMA | bis-EMA + 5 wt % multiPOSS | bis-EMA + 10 wt % multiPOSS | bis-EMA + 15 wt % multiPOSS |
|---|---|---|---|---|
| AIBN initiator (4 h 80 °C + 2 h 130 °C) | 83 | 82 | 79 | 75 |
| tBPO initiator (4 h 130 °C) | 93 | 91 | 87 | 82 |

**Table 3. WLF Parameters, *T*α, and Rubbery Modulus of Methacrylate Networks Including $^{i}$BuPOSS and CyPOSS as Pendant Groups**

| | $C^g_1$ | $C^g_2$ [K] | $10^2 f_g/B$ | $10^4 \alpha_f/B$ | *T*α [°C] at 1 Hz | rubbery modulus at *T*α + 50 °C [MPa] |
|---|---|---|---|---|---|---|
| bis-EMA/CHMA(50/50) | 10.6 ± 0.5 | 97.2 ± 4.5 | 4.1 ± 0.2 | 4.2 ± 0.4 | 113 | 22.5 |
| +5% $^{i}$BuPOSS | 9.8 ± 0.5 | 89.8 ± 4.6 | 4.4 ± 0.2 | 4.9 ± 0. 4 | 110 | 19.5 |
| +10% $^{i}$BuPOSS | 10.2 ± 0.5 | 87.6 ± 4.3 | 4.3 ± 0.2 | 4.9 ± 0.5 | 110 | 18.0 |
| +5% CyPOSS | 10.6 ± 0.6 | 99.7 ± 5.8 | 4.1 ± 0.2 | 4.1 ± 0.5 | 112 | 19.4 |
| +10%CyPOSS | 10.3 ± 0.5 | 92 ± 4.2 | 4.2 ± 0.3 | 4.6 ± 0.4 | 113 | 21.3 |
| bis-EMA/CHMA(10/90) | 9.1 ± 0.4 | 103.7 ± 4.6 | 4.8 ± 0.2 | 4.6 ± 0.4 | 117 | 1.9 |
| +10% $^{i}$BuPOSS | 7.7 ± 0.6 | 87.9 ± 6.8 | 5.6 ± 0.4 | 6.4 ± 1.0 | 111 | 1.5 |
| +10% CyPOSS | 8.6 ± 0.5 | 95.6 ± 5.6 | 5.0 ± 0.4 | 5.3 ± 0.7 | 118 | 2.0 |

can be related to the free volume fraction, $f_0$, and the free volume expansion coefficient, $\alpha_f$, from the Doolittle's theory, through the following relationships:[32]

$$C^0_1 = \frac{B}{2.303 f_0} \quad (2)$$

$$C^0_2 = \frac{f_0}{\alpha_f} \quad (3)$$

*B* is a constant, which is considered most of the time to be unity.

WLF coefficients were determined by plotting $(T - T_0)/\log(a_T)$ against $(T - T_0)$: the coefficient $C^0_1$ was obtained from the slope which is $-1/C^0_1$ and the coefficient $C^0_2$ from the intersection at $T = T_0$ which is $-C^0_2/C^0_1$. A representative WLF plot for the Bis-EMA/CHMA (50/50) networks, unmodified and modified with 5 and 10 wt % of $^{i}$BuPOSS is shown in Figure 9. In each case, a linear dependence is obtained. Once $C^0_1$ and $C^0_2$ were known, the WLF parameters at a same $T_g$ (chosen as 108.5 °C), $C^g_1$ and $C^g_2$, were calculated thanks to eqs 4 and 5:[18,32]

$$T_0 - C^0_2 = T_g - C^g_2 \quad (4)$$

$$C^0_1 C^0_2 = C^g_1 C^g_2 \quad (5)$$

Finally, $f_g$ and $\alpha_f$ were determined from $C^g_1$ and $C^g_2$ using eqs 2 and 3.

Table 3 provides a summary of WLF parameters, $f_g$ and $\alpha_f$, as well as $T_g$ and the rubbery modulus of all networks based on Bis-EMA/CHMA (50/50) + POSS and Bis-EMA/CHMA (10/90) + POSS. However, due to the low accuracy of WLF coefficients, only a qualitative interpretation from these values can be given.

Networks modified with $^{i}$BuPOSS have higher fg and $\alpha_f$ as compared to the reference network whatever the Bis-EMA/CHMA ratio. Then, to explain the slight decrease of rubbery modulus induced by $^{i}$BuPOSS, one can note the following factors:

(i) $^{i}$BuPOSS is a monofunctional monomer that acts as a chain extender causing the average cross-linking density to decrease.

(ii) $^{i}$BuPOSS is a nanometer scale monomer occupying a large volume that is no longer available for cross-links. The average number of cross-links per volume tends to be reduced.

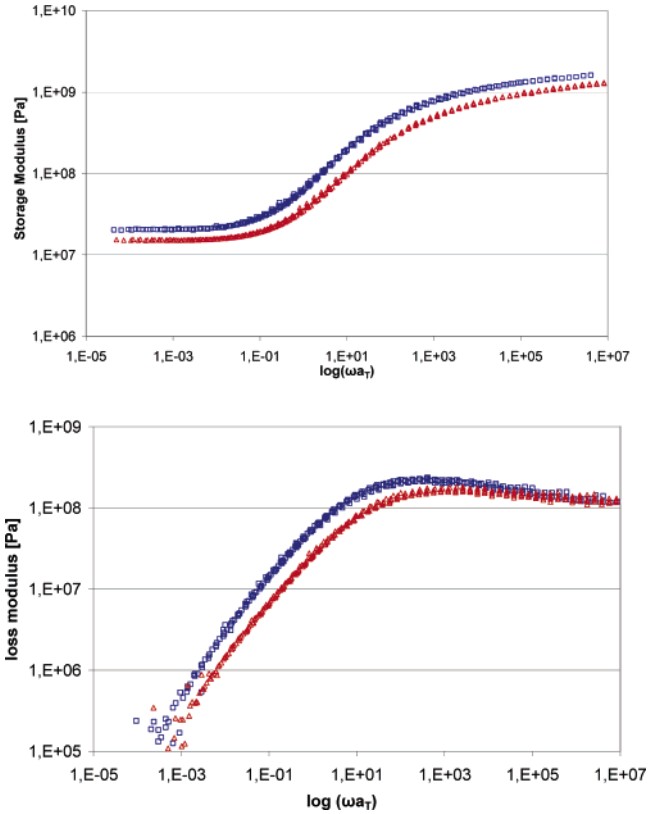


**Figure 8.** (top) Master curves for the storage modulus. (bottom) Master curves for the loss modulus. $T_0$ = 108.5 °C. Bis-EMA/CHMA (50/50) (□); Bis-EMA/CHMA (50/50) + 10% $^{i}$BuPOSS (○). Curing cycle: 8 h 65 °C + 2 h 130 °C.

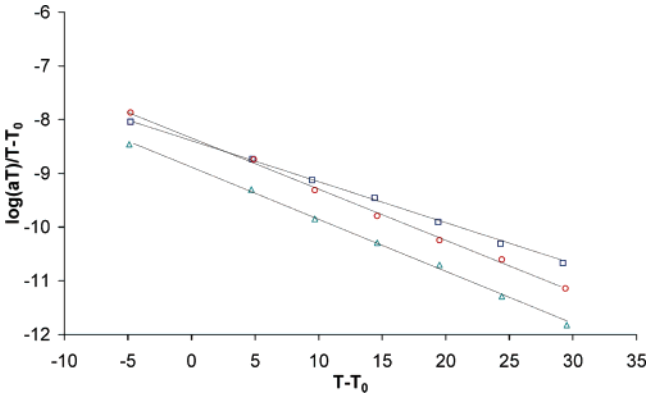


**Figure 9.** WLF plot from shift factors, $a_T$: Bis-EMA/CHMA (50/50) (□); Bis-EMA/CHMA (50/50) + 5 wt % $^{i}$BuPOSS (△); Bis-EMA/CHMA (50/50) + 10 wt % $^{i}$BuPOSS (○).

(iii) Disordering of the crystalline domains which are not covalently linked to the network takes place; this disordering occurs above $T_m$ ($^i$BuPOSS) and leads to liquid droplets of $^i$BuPOSS in the rubbery matrix

Besides this, the increase of free volume expansion coefficient in the presence of $^i$BuPOSS is consistent with a decrease of average cross-linking density.[33]

The lower $T\alpha$ can be explained by the following: (i) the increase of free volume fraction coming from the lower cross-linking density and the fact that $^i$BuPOSS is a bulky monomer making the packing of polymer chains around these nano-objects difficult; (ii) the plasticizing effect of $^i$BuPOSS due to the isobutyl ligands.

Then, $^i$BuPOSS has effects that tend to increase molecular mobility (decrease of cross-linking density, increase of free volume fraction, and plasticizing effect). Figure 8 illustrates this influence in the case of the network Bis-EMA/CHMA (50/50) + 10 wt % $^i$BuPOSS. The master curve of the storage modulus as a function of frequency at $T_0 = 108.5$ °C is shifted toward higher frequencies as compared to the pure matrix. This indicates the existence of shorter relaxation times in the presence of $^i$BuPOSS. However, it is well-known that POSS incorporated as pendant groups are massive and bulky monomers that slow molecular motions (POSS = "anchor object").[34] As a consequence, at loadings below 10 wt % of $^i$BuPOSS, effects leading to an increase of molecular mobility overcome the "anchor" effect.

The addition of CyPOSS to the networks up to 10 wt % does not modify the thermomechanical behavior of the material as confirmed by the low influence on the WLF parameters. In this case the large crystalline domains that were found using WAXS and TEM remain stable as the temperature is increased, because their melting temperature is very high. However these domains, which we can see as micrometer-size filler, do not bring any enhancement of the viscoelastic properties of the network. No change of molecular mobility is observed as most of the CyPOSS clusters are not included in polymer chains.

### 2. Networks with POSS as Cross-Links

A significant influence of the addition of multiPOSS to Bis-EMA is observed on the final double bond conversion: increasing the POSS content leads to a small decrease of the conversion due to steric hindrance associated with the high functionality of these nano-objects (Table 2). This effect is higher than for the monofunctional POSS (Table 1).

The networks including multiPOSS as a cross-linking point are fully amorphous as shown by the absence of sharp crystalline reflections in the WAXS profiles depicted in Figure 10. This result was expected because the multiPOSS monomer is liquid. The multiPOSS are well dispersed in the organic medium, at a molecular scale, as there is no sign of any assembling of POSS within the network. This conclusion is confirmed by the TEM micrographs which show no silicon-rich zone even at high magnification. This excellent dispersion is explained by the combination of three factors: (i) the high solubility of multiPOSS in the Bis-EMA monomer, (ii) the reactivity of the methacrylate group borne by POSS molecule, which is slightly lower than the ones of Bis-EMA, so that POSS can be incorporated in the network at the early stage of the polymerization, and (iii) its high functionality, which prevents self-organization of POSS. However, this situation is not general: in some cases, similar results were found in the literature,[2] but in other cases, aggregates were observed.[9,10,35,36]

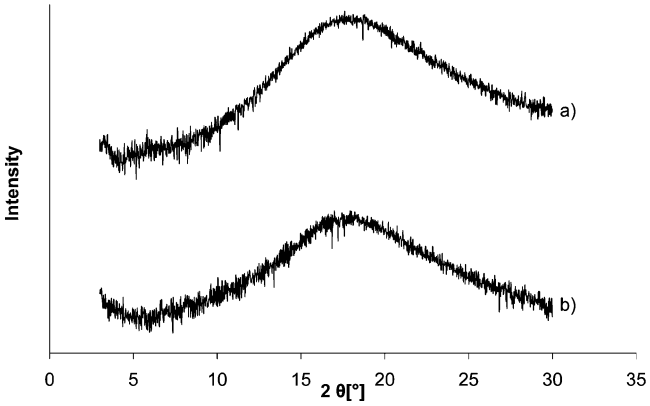


**Figure 10.** WAXS patterns: (a) Bis-EMA; (b) Bis-EMA + 15 wt % multiPOSS.

An increase in the rubbery modulus with increasing multiPOSS content is observed as shown in Figure 11a. This modulus is related to the average cross-link density which increases with rising amounts of multiPOSS, despite the lower final conversion of double bonds. As an example, the incorporation of 15 wt % of multiPOSS leads to an increase of 53 MPa of the rubbery modulus. A decrease of the magnitude of tan $\delta$ is also noticed, it is accompanied by an increase in the width of the glass transition region (Figure 11b). It is well-known that networks synthesized by chain polymerization result from the agglomeration of highly cross-linked microgel particles, with high $T_g$ region located in the core of microgels and inter microgel regions with a lower $T_g$. The broad tan $\delta$ peak observed on the Bis-EMA matrix could be explained by the different associated relaxation processes.[37] Adding multiPOSS increases the network heterogeneity in terms of molecular mobility, because of its high functionality. During the polymerization, the presence of multiPOSS leads to a local double bond concentration around the growing macroradical higher than in the neat Bis-EMA network. Therefore, we believe that Bis-EMA/multiPOSS systems have a higher tendency to form microgels and a broader distribution of relaxation times of the resulting network is obtained.

To reduce this broadening of the distribution of relaxation times and also to increase the final double bond conversion, we decided to synthesize Bis-EMA/multiPOSS at a polymerization temperature higher than the final glass transition temperature; 130 °C was chosen and tertiobutyl peroxide, $^t$BPO, initiator was used instead of AIBN. Polymerization time was 4 h. The values of final double bond conversion are reported in Table 2. In all cases higher conversions are obtained, the increase being 7 to 10%. This effect results from the higher polymerization temperature that facilitates the diffusion of reactive species. Of course, as shown in Figure 12, this increase of conversion has a clear consequence on the value of $T\alpha$ and rubbery modulus which both show a significant increase. Moreover the shape of the tan $\delta$ peak is different; it is narrower than the one of the network initiated by AIBN. This effect is also visible on the neat matrix (Figure 13): an increase of 16 MPa and of 20 °C in the value of $T\alpha$ is obtained when $^t$BPO is used instead of AIBN. As previously noted, increasing the weight fraction of multiPOSS in the organic matrix considerably increases the rubbery modulus as can be seen in Figure 13: an increase of 120 MPa is found for Bis-EMA + 15 wt % multiPOSS + $^t$BPO. Despite this effect, any significant change of $T\alpha$ occurs in the presence of multiPOSS. In fact, what is really important to note is the broadening of the relaxation processes at high temperatures induced by multiPOSS as

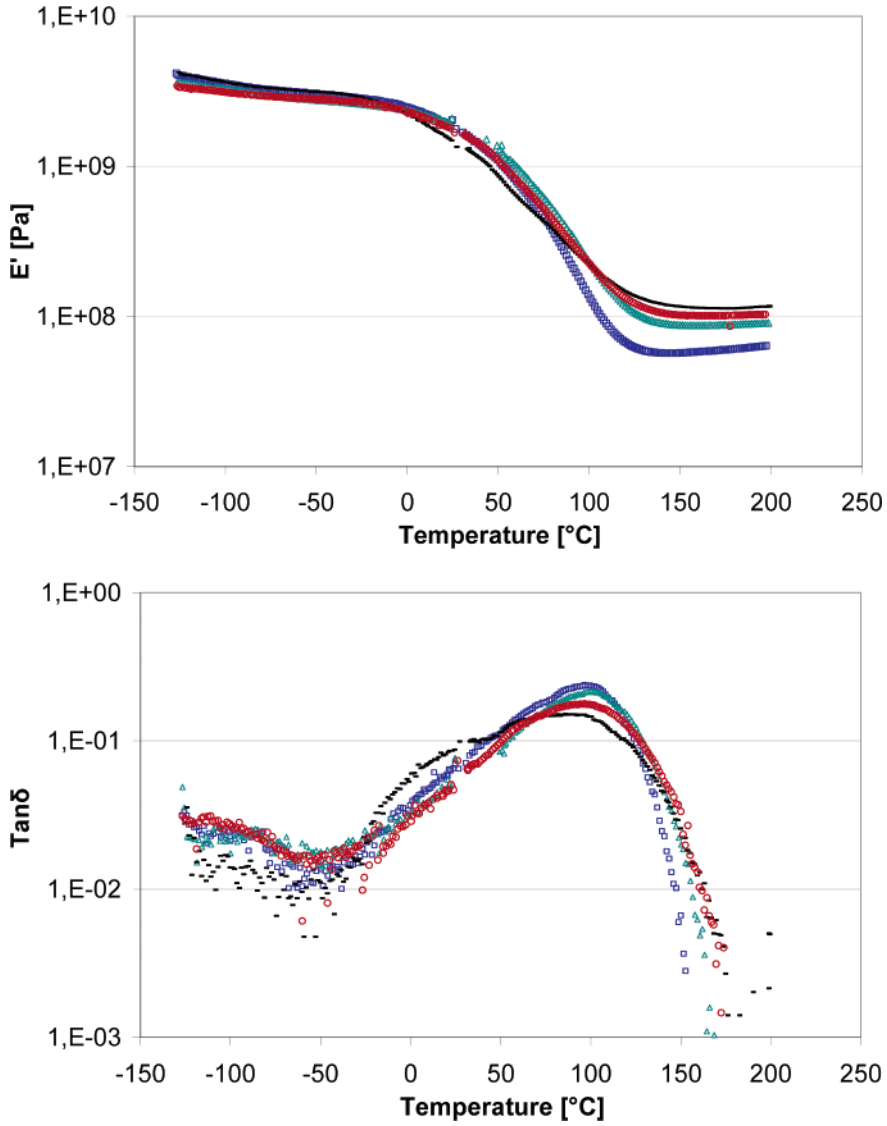


**Figure 11.** Influence of multiPOSS weight fraction on storage modulus, $G'$ (a), and loss factor, tan $\delta$ (b), at 1 Hz: Bis-EMA (□); Bis-EMA + 5 wt % multiPOSS (△); Bis-EMA + 10 wt % multiPOSS (○); Bis-EMA+ 15 wt % multiPOSS (×) 8 h 80 °C + 2 h 150 °C.

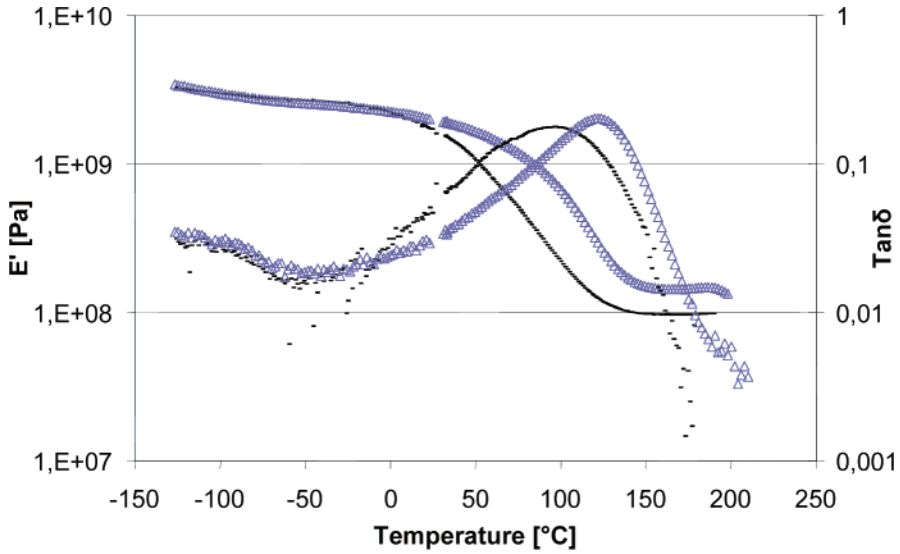


**Figure 12.** Influence of polymerization temperature on storage modulus, $G'$, and loss factor, tan $\delta$, at 1 Hz: (△) Bis-EMA + 10 wt % multiPOSS + $^t$BPO; 4 h at 130 °C (−) Bis-EMA + 10 wt % multiPOSS + AIBN; 4 h at 80 °C + 4 h at 130 °C.

observed elsewhere.[36] This can be attributed to both the increased average cross-linking density and the fact that many chains are linked to a bulky and highly functional POSS cage having a low mobility.

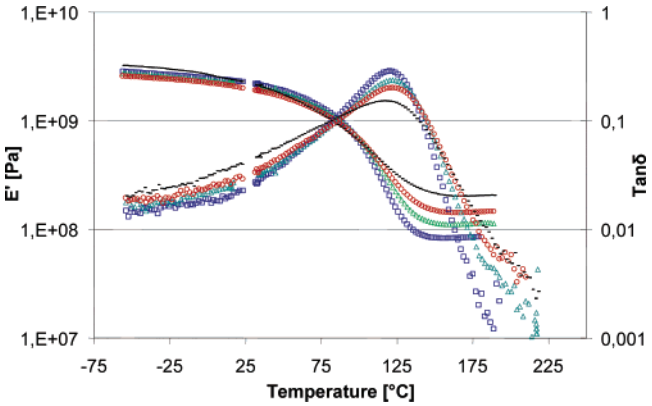


**Figure 13.** Influence of multiPOSS wt % and $^t$BPO initiator on storage modulus, $G'$ (a), and loss factor, tan $\delta$ (b), at 1 Hz: Bis-EMA (□); Bis-EMA + 5 wt % multiPOSS (△); Bis-EMA + 10 wt % multiPOSS (○); Bis-EMA + 15 wt % multiPOSS (×), 4 h at 130 °C.

## Conclusions

Two types of monofunctional and one type of multifunctional polyhedral oligomeric silsesquioxanes were employed to prepare hybrid I/O networks, i.e., POSS-containing dimethacrylate networks. The different materials were characterized using wide-angle X-ray scattering, electron microscopy, and dynamic mechanical spectroscopy.

The free radical copolymerization between a POSS bearing eight methacrylate groups and a dimethacrylate monomer leads to very well dispersed clusters at the molecular scale. This excellent dispersion is the result of the very good miscibility of multiPOSS into the organic monomer and of its high functionality which prevents phase separation during the polymerization. The nanostructuration of monofunctional POSS is more complex. This type of nanocluster shows a high tendency to phase separate and to form crystalline domains during polymerization. To have an initially soluble POSS in the dimethacrylate monomer a reactive diluent is required, but it does not prevent the phase separation of the nanocluster as reaction occurs. This effect is clearly more pronounced with cyclohexyl POSS as compared to isobutyl POSS, due to the stronger POSS−POSS interactions in the first case. Moreover it was also demonstrated that most of the monofunctional POSS were not covalently bonded to the network.

The multifunctional POSS behaves as a cross-linking agent; i.e., it increases the average cross-link density and as a consequence increases the value of the rubbery modulus. However, the $T_g$, estimated from DMS, of the hybrid networks is not affected, and only a broadening of the transition was observed as the amount of POSS was increased. The dispersion at a molecular scale of multiPOSS clusters coupled with the high functionality of these objects enables us to state that each multiPOSS molecule acts as an individual cross-link. Monofunctional POSS does not bring any specific reinforcement effect to the network at loading below 10 wt %; some are included as pendant groups in the network, but this does not lead to any strong change in the value of $T_g$ or modulus.

We believe that methacrylate-functionalized POSS can be expected to improve the properties of dimethacrylate-based networks in the field of surface properties,[16] optical properties and shrinkage,[15] rather than in the field of mechanical properties.

**Acknowledgment.** This work was supported by the French Ministry of Education and by the European Community through Research Training Networks, funded under the 6th framework program, under Contract HPRN-CT-2002-00306 "NBB-HYBRIDS".

## References and Notes

(1) Provatas, A.; Matisons, J. G. *Trends Polym. Sci.* **1997**, *5*, 327.
(2) Li, G. Z.; Wang, L. C.; Ni, H. L.; Pittman, C. U. *J. Inorg. Organomet. Polym.* **2001**, *11*, 123.
(3) Lee, A.; Lichtenhan, J. D. *Macromolecules* **1998**, *31*, 4970.
(4) Lee, A.; Lichtenhan, J. D. *J. Appl. Polym. Sci.* **1999**, *73*, 1993.
(5) Choi, J.; Harcup, J.; Yee, A. F.; Zhu, Q.; Laine, R. M. *J. Am. Chem. Soc.* **2001**, *123*, 11420.
(6) Laine, R. M.; Choi, J.; Lee, I. *Adv. Mater.* **2001**, *13*, 800.
(7) Abad, M. J.; Barral, L.; Fasce, D. F.; Williams, R. J. J. *Macromolecules* **2003**, *36*, 3128.
(8) Choi, J.; Kim, S. G.; Laine, R. M. *Macromolecules* **2004**, *37*, 99.
(9) Matejka, L.; Strachota, L.; Plestil, J.; Whelan, P.; Steinhart, M.; Slouf, M. *Macromolecules* **2004**, *37*, 9449.
(10) Strachota, A.; Kroutilova, I.; Kovarova, J.; Matejka, L. *Macromolecules* **2004**, *37*, 9457.
(11) Mya, K. Y.; He, C.; Huang, J.; Xiao, Y.; Dai, J.; Siow, Y. P. *J. Polym. Sci., Part A: Polym. Chem.* **2004**, *42*, 3490.
(12) Ni, Y.; Zheng, S.; Nie, K. *Polymer* **2004**, *45*, 5557.
(13) Pittman, C. U., Jr.; Li, G.-Z.; Ni, H. *Macromol. Symp.* **2003**, *196*, 301.
(14) Li, G. Z.; Cho, H.; Wang, L.; Toghiani, H.; Pittman, C. U., Jr. *J. Polym. Sci., Part A Polym. Chem.* **2005**, *43*, 355.
(15) Gao, F.; Tong, Y.; Schricker, S. R.; Cubertson, B. M. *Polym. Adv. Technol.* **2001**, *12*, 355.
(16) Bizet, S. Ph.D. Thesis, INSA Lyon, 2004; 04 ISAL 0099.
(17) Bizet, S.; Galy, J.; Gérard, J. F. Presented at IUPAC Macro 2004, Paris.
(18) Kopesky, E. T.; Haddad, T. SR. E.; Cohen, R. E.; McKinley, G. H. *Macromolecules* **2004**, *37*, 8992.
(19) Li, G. Z.; Wang, L.; Toghiani, H.; Daulton, T. L.; Pittman, C. U., Jr. *Polymer* **2002**, *43*, 4167.
(20) Dusek, K. *Collect. Czech. Chem. Commun.* **1993**, *58*, 2245.
(21) Dusek, K. *Polym. Gels Networks* **1996**, *4*, 383.
(22) Dusek, K. *Angew. Makromol. Chem.* **1996**, *240*, 1.
(23) Zhu, S.; Hamielec, A. E. *Makromol. Chem., Macromol. Symp.* **1992**, *63*, 135.
(24) Anseth, K. S.; Bowman, C. N. *J. Polym. Sci., Part B: Polym. Phys.* **1995**, *33*, 1769.
(25) Anseth, K. S.; Anderson, K. J.; Bowmann, C. N. *Makromol. Chem. Phys.* **1996**, *197*, 833.
(26) Rey, L.; Galy, J.; Sautereau, H. *Macromolecules* **2000**, *33*, 6780.
(27) Hybrid Plastics, www.hybridplastics.com.
(28) Rey, L.; Galy, J.; Sautereau, H.; Lachenal, G.; Henry, D.; Vial, J. *J. Appl. Spectrosc.* **2000**, *54*, 39.
(29) Moore, B. M.; Haddad, T. S.; Gonzalez, R. I.; Schlaefer, C. *Polym. Prepr.* **2004**, *45*, 692.
(30) Miler, R. L.; Boyer R. F. *J. Polym. Sci., Part B: Polym. Phys.* **1984**, *22*, 2021.
(31) Ribes-Greus, A.; Gomez-Ribelles, J. L.; Diaz-Calleja, R. *Polymer* **1985**, *26*, 1849.
(32) Ferry, J. D. *Viscoelastic properties of polymers*, 3rd ed; John Wiley & Sons: New York, 1980.
(33) Gérard, J. F.; Galy, J.; Pascault, J.-P. *Polym. Eng. Sci.* **1991**, *31*, 615.
(34) Romo-Uribe, A.; Mather, P. T.; Haddad T. S.; Lichtenhan, J. D. *J. Polym. Sci., Part B: Polym. Phys.* **1998**, *36*, 1857.
(35) Kim, G. M.; Qin, H.; Fang, X.; Sun, F. C.; Mather, P. T. *J. Polym. Sci., Part B: Polym. Phys.* **2003**, *41*, 3299.
(36) Li, G. Z.; Wang, L.; Toghiani, H.; Daulton, T. L.; Koyama, K.; Pittman, C. U. *Macromolecules* **2001**, *34*, 8686.
(37) Rey, L.; Galy, J.; Sautereau, H. *Polym. Int.* **2004**, *53*, 557.

MA051574X